Disordered CuN_6 Jahn−Teller Centers in Hexakis(1-methyltetrazole)copper(II) Tetrafluoroborate: A Temperature-Dependent X-ray Diffraction and EPR Study

Paul E. M. Wijnands,[1a,c] John S. Wood,*[,1b] Jan Reedijk,[1a] and Wim J. A. Maaskant*[,1a]

Gorlaeus Laboratories, Leiden Institute of Chemistry, Leiden University, P.O. Box 9502, 2300 RA Leiden, The Netherlands, and Department of Chemistry, Box 34510, University of Massachusetts, Amherst, Massachusetts 01003-4510

Received March 16, 1995[⊗]

The influence of the molecular crystalline arrangement upon the state of a Jahn−Teller-active center has been investigated in crystals of the complex $Cu(mtz)_6(BF_4)_2$, where mtz = 1-methyltetrazole. Crystal structures at 293, 123, and 93 K were determined by X-ray diffraction for the copper complex and at 293 and 100 K also for the analogous zinc complex, $Zn(mtz)_6(BF_4)_2$. The respective lattice parameters for the copper complex at 293, 123, and 93 K are as follows: a = 18.137(4), 17.597(4), 17.575(4) Å; b = 10.247(4), 10.131(4), 10.133(4); c = 18.446(5), 18.531(4), 18.535(4) Å; β = 112.62(2), 113.55(2), 113.61(2)°. Those for the zinc complexes at 293 and 100 K, respectively, are as follows: a = 18.153(2), 17.663(2) Å; b = 10.289(1), 10.159(2) Å; c = 18.506(3), 18.578(3) Å; β = 113.21(1), 114.15(2)°. The crystal system is monoclinic, space group $P2_1/n$ (Z = 4), for all crystals with two crystallographically inequivalent pairs of centrosymmetric molecules, $M(mtz)_6(BF_4)_2$, in the unit cell. The two inequivalent $Cu(mtz)_6^{2+}$ complexes, Cu(A) and Cu(B), both exhibit Jahn−Teller distortions, but in different ways, the Cu−N distances for the unit on site A being 2.015(4), 2.031(5), and 2.384(5) Å at 93 K, while those for the unit on site B are 2.053(5), 2.126(5), and 2.204(5) Å. However, the Jahn−Teller radii of the two complexes, as calculated from the metal−ligand distances and the **U** tensors of the two CuN_6 units, were both found to be 0.41(3) Å. EPR experiments at room temperature on polycrystalline samples of the pure copper compound and of the copper-doped zinc compound confirm the presence of two different Jahn−Teller centers; both complexes are rapidly pulsating, but the CuN_6 units on site A are confined predominantly to one potential well of the warped Mexican hat potential, whereas the CuN_6 units on site B have density in all three wells. At 78 K, however, the spectrum of the polycrystalline material is consistent with a single site having an axial **g** tensor with maximum anisotropy ($g_\parallel$ = 2.300(5), $g_\perp$ = 2.068(5)). While the low-temperature X-ray results also indicate a structure in which the Cu(A) center is exclusively populated in one potential well, the **U** tensor and potential well population data for the Cu(B) centers indicate that at 93 K a nonpulsating averaged structure based on tetragonally elongated CuN_6 units is being observed. The more pronounced preference for the CuN_6 octahedron on site A to show elongation in one specific direction, in contrast to that on the B site, appears to be due to the differing impacts of the local-site strains at the two distinct centers of symmetry, and a simple model for evaluating a crystal "packing" strain from the bond length data for the isomorphous zinc complex is described.

Introduction

Metal complexes with a variety of tetrazole ligands were first synthesized by Franke.[2] Some of these exhibit interesting physical behavior; for example, one of these compounds, $Fe(mtz)_6(BF_4)_2$, mtz = 1-methyltetrazole, has been shown to display a new type of spin transition,[3] and as will be seen in the present paper, X-ray experiments on $Cu(mtz)_6(BF_4)_2$ give evidence of two inequivalent $Cu(mtz)_6^{2+}$ centers, both of which are required to have inversion symmetry. Initial room-temperature X-ray studies on the copper complex had indicated that the centers are subject to different Jahn−Teller effects. Therefore, in order to obtain more precise information about the Jahn−Teller states of the two centers, extensive temperature-dependent X-ray diffraction measurements were undertaken on the copper complex and the isomorphous zinc compound. In addition, EPR experiments on pure and on copper-doped $Zn(mtz)_6(BF_4)_2$ have been carried out, and a preliminary communication dealing with part of the EPR work has appeared previously.[4] There are several other literature examples of copper(II) complexes containing two crystallographically inequivalent Jahn−Teller-active centers, namely, $Cu(hb(pz)_3)_2$[5] [$hb(pz)_3$ = hydrotris(pyrazolyl)borate], $Cu(en)_3Cl_2 \cdot {}^3/_4en$[6] (en = 1,2-ethylenediamine), $Cu(Et\text{-}cPO)_2$[7] [Et−cPO = cyclopentadienyl)tris(diethyl phosphito-*P*)cobaltate ion], $[Cu(H_2O)_6](bs)_2$[8] (bs = benzenesulfonate), and very recently $Cu(ttcn)_2(BF_4)_2 \cdot 2MeCN$[9] (ttcn = trithiacyclononane). However, this appears to be the first example where an attempt has been made to understand the difference between the two centers in terms of the local-site strains arising from the crystal packing.

⊗ Abstract published in *Advance ACS Abstracts,* February 1, 1996.

(1) (a) Leiden University. (b) University of Massachusetts. (c) Present address: E. I. du Pont de Nemours and Co., P.O. Box 145, 3300 AC Dordrecht, The Netherlands.
(2) Franke, P. L.; Groeneveld, W. L. *Transition Met. Chem.* **1981**, *6*, 54. Franke, P. L. Ph.D. Thesis, Leiden University, 1982.
(3) Poganiuch, P.; Decurtins, S.; Gutlich, P. *J. Am. Chem. Soc.* **1990**, *112*, 3270.
(4) Wijnands, P. E. M.; Maaskant, W. J. A.; Reedijk, J. *Chem. Phys. Lett.* **1986**, *130*, 536.
(5) Murphy, A.; Hathaway, B. J.; King, T. J. *J. Chem. Soc., Dalton Trans.* **1979**, 1646.
(6) Bertini, I.; Dapporto, P.; Gatteschi, D.; Scozzafava, A. *J. Chem. Soc., Dalton Trans.* **1979**, 1409.
(7) Dubler, E.; Linovsky, L.; Klaui, W. *Transition Met. Chem.* **1979**, *4*, 191.
(8) Couldwell, C.; Prout, K.; Robey, D.; Taylor, R.; Rossoti, F. J. C. *Acta Crystallogr.* **1978**, *B34*, 1491.
(9) Glass, R. S.; Steffen, L. K.; Swanson, D. D.; Wilson, G. S.; de Gelder, R.; de Graaff, R. A. G.; Reedijk, J. *Inorg. Chim. Acta* **1993**, *207*, 241.

0020-1669/96/1335-1214$12.00/0

Table 1. Crystallographic Data for $Cu(mtz)_6(BF_4)_2$ at 293, 123, and 93 K and for $Zn(mtz)_6(BF_4)_2$ at 293 and 100 K

	empirical formula				
	$CuC_{12}H_{24}N_{24}B_2F_8$			$ZnC_{12}H_{24}N_{24}B_2F_8$	
mol wt	741.65	741.65	741.65	743.5	743.5
temp (K)	293	123	93	293	100
space group	$P2_1/n$	$P2_1/n$	$P2_1/n$	$P2_1/n$	$P2_1/n$
Z	4 (2 independent centrosymmetric molecules)				
a (Å)	18.137(4)	17.597(4)	17.575(4)	18.153(2)	17.663(7)
b (Å)	10.247(4)	10.131(4)	10.133(4)	10.289(1)	10.159(3)
c (Å)	18.446(5)	18.531(4)	18.535(4)	18.506(3)	18.578(4)
β (deg)	112.62(2)	113.55(2)	113.61(2)	113.21(1)	114.15(2)
vol (Å^3)	3164(3)	3028(3)	3025(3)	3177(2)	3042(3)
calcd density (g/cm^3)	1.56	1.63	1.63	1.55	1.61
obsd density (g/cm^3)				1.52	
μ (cm^{-1})	8.25			8.8	
radiation λ (Å)	0.710 73	0.710 73	0.710 73	0.710 73	0.710 73
R[a]	0.060	0.046	0.045	0.077	0.043
R_w[b]	0.080	0.049	0.049	0.099	0.058

[a] $R = \sum||F_o| - |F_c||/\sum|F_o|$. [b] $R_w = (\sum w(|F_o| - |F_c|)^2/\sum w|F_o|^2)^{1/2}$.

From a more general evaluation of crystals of hexacoordinated copper(II) compounds,[10] it invariably turns out that the Jahn−Teller-active metal centers are subject to a strong $E \otimes \epsilon$ coupling resulting in appreciable warping of the Mexican hat potential energy surface.[11] The three resulting minima may have differing energies, but the locations within the so-called Jahn−Teller triangle are, in most instances, still close to $\phi = 0$, $2\pi/3$, and $4\pi/3$ radians, where the angular coordinate ϕ describes the orientations of the distorted octahedra. These energy minima are represented by octahedra, tetragonally elongated along *x*, *y*, and *z*, respectively, and the properties of many of these complexes can be treated according to a dynamic equilibrium between the mimima. Both the frequency of transitions between the energy minima and the populations of the differently elongated octahedra may be temperature dependent, and while EPR experiments can give information on both of these, X-ray diffraction experiments only show the population distribution. The above description certainly applies to $Cu(mtz)_6(BF_4)_2$, since the variable-temperature EPR measurements on powder and single-crystal samples[4] give a single nearly axially symmetric **g** tensor for both inequivalent CuN_6 centers, consistent with tetragonally elongated geometries, despite the low-symmetry crystalline fields at the copper atoms. Likewise the X-ray structural results for $Cu(mtz)_6(BF_4)_2$ are also in accord with this description.

Experimental Section

Synthesis of the Complexes. Hexakis(1-methyltetrazole)copper(II) bis(tetrafluoroborate) and the analogous zinc(II) compound were synthesized as described by Franke.[2] Platelike crystals were grown from a 1:1 ethanol−water solution after standing in air for about 3 months. Copper-doped zinc complexes were synthesized by adding a small amount of $Cu(BF_4)_2$ to solutions containing Zn^{2+} ions and the ligands. Because of the presence of the tetrazole ligands, these compounds can explode relatively easily upon thermal or mechanical shock.

X-ray Determination and Refinement. X-ray data were collected on a CAD-4 (Enraf-Nonius) diffractometer using graphite-monochromated Mo K_α radiation for a crystal of the copper complex, at 293, 123, and 93 K and for a crystal of the zinc complex at 293 and 100 K. Crystal cooling was achieved with a locally modified Enraf-Nonius liquid-nitrogen flow system; the temperature control was ±1 K. The crystals used for X-ray work had dimensions of about 0.4 × 0.35 × 0.15 mm and were mounted approximately along the *b* axis. The same crystal was used for both room- and low-temperature measurements in each instance. Unit cell parameters and related information are given in Table 1, while more complete information on the data collection is given in the Supporting Information. On the basis of the results of Ψ scans of several reflections, which indicated a maximum variation in their transmission factors of approximately 5%, absorption corrections were considered to be rather small and were omitted. The solution of the 293 K structure of the copper complex was carried out by standard heavy-atom procedures, with the package of programs written or modified for the Leiden University computer.[12] The structure was refined by full-matrix least squares with atomic scattering factors for the non-hydrogen atoms taken from ref 13. Corrections for anomalous dispersion were included.[14] The function minimized was $\Sigma w(|F_o| - |F_c|)^2$, where $w^{1/2} = 1/\sigma(F)$. The atomic coordinates and modified equivalent isotropic temperature factors from the room-temperature copper structure were used as starting parameters for the refinement of all other data sets. As anticipated, the tetrafluoroborate anions had large **U** tensors, indicative of extensive librational motion for these ions, particularly the $BF_4(2)$ group. While difference Fourier maps showed many residual peaks of significant density at normal B−F distances, normal Fourier maps did not suggest more than one orientation for each of the two independent anions. Accordingly, in order to best model the statistical averaging, the fluorine density of both BF_4 groups for the room-temperature data sets was divided into two parts, namely a spherically averaged shell having a fixed radius of 1.42 Å whose center was constrained to lie on the boron atom plus four conventional fluorines with reduced and equal occupancy factors. These atoms were allowed to refine independently. The occupancy of each fluorine atom, i.e., the conventional plus the spherical component, was constrained to unity. For the low-temperature data sets, only $BF_4(2)$ for the copper complex was refined by this method. For the zinc complex, both BF_4 groups were refined conventionally. Hydrogen atoms were located from difference Fourier maps, and in the case of the low-temperature data sets, their positions were refined. The atomic scattering factor for hydrogen used is that given by Stewart et al.[15] All calculations with the modified model for the anions were carried out using the program LINEX.[16] The fractional atomic coordinates and U_{eq} values for all the non-hydrogen atoms of all five structures are listed in the Supporting Information.

EPR measurements were carried out on Varian E-3 (X-band) and E-12 (Q-band) spectrometers on different samples as follows: (1) measurements at X-band on crystalline samples of the pure copper compound between 4 and 450 K and Q-band measurements on the

(10) Wijnands, P. E. M. Ph.D. Thesis, University of Leiden, 1989. Copies of the thesis are available upon request from P.E.M.W. Address: see ref 1c.

(11) Reinen, D.; Friebel C. *Struct. Bonding* **1979**, *37*, 1.

(12) Programs written by R. A. G. de Graaff and E. Rutten-Keulemans, Leiden University.

(13) *International Tables for X-Ray Crystallography*; Kynoch Press: Birmingham, England, 1974; Vol. IV.

(14) Cromer, D. T.; Liberman, D. *J. Chem. Phys.* **1970**, *53*, 1891.

(15) Stewart, R. F.; Davidson, R. F.; Simpson, W. T. *J. Chem. Phys.* **1965**, *42*, 3175.

(16) Busing, W. R.; Martin, K. O.; Levy, H. A. ORFLS. Report ORNL-TM-305; Oak Ridge National Laboratory: Oak Ridge, TN, 1962.

Table 2. Fractional Coordinates and U_{eq} Values for the Centrosymmetric MN_6 Groups: $Cu(mtz)_6(BF_4)_2$ at 293 K (First Lines), 123 K (Second Lines), and 93 K (Third Lines); $Zn(mtz)_6(BF_4)_2$ at 293 K (Fourth Lines) and 100 K (Fifth Lines)

	10^4x	10^4y	10^4z	U_{eq}[a] (10^{-3} Å^2)
M(A)	0	0	0	39(1)
	0	0	0	16(1)
	0	0	0	16(1)
	0	0	0	43(2)
	0	0	0	14(1)
N41(A)	−843(5)	488(8)	−1289(5)	47(5)
	−874(3)	529(5)	−1324(3)	29(3)
	−880(3)	535(5)	−1323(3)	18(3)
	−806(6)	474(11)	−1201(6)	38(8)
	−821(2)	507(3)	−1220(2)	16(1)
N42(A)	−656(5)	1121(7)	431(5)	40(5)
	−673(3)	1117(5)	425(3)	18(3)
	−677(3)	1111(5)	425(3)	16(3)
	−688(7)	1201(11)	448(7)	44(8)
	−724(2)	1174(3)	429(2)	16(1)
N43(A)	722(5)	1595(8)	4(5)	44(5)
	719(3)	1589(5)	21(3)	17(3)
	720(3)	1583(5)	17(3)	15(3)
	764(7)	1638(12)	20(7)	44(8)
	764(2)	1668(3)	30(2)	15(1)
M(B)	5000	0	0	58(1)
	5000	0	0	26(1)
	5000	0	0	26(1)
	5000	0	0	64(2)
	5000	0	0	22(1)
N41(B)	4168(7)	−391(10)	520(6)	66(7)
	4108(4)	−462(6)	527(3)	34(4)
	4103(4)	−458(6)	527(3)	33(4)
	4162(8)	−426(14)	533(8)	63(10)
	4131(2)	−460(3)	520(2)	22(1)
N42(B)	4369(6)	−1190(10)	−953(5)	63(7)
	4386(3)	−1197(5)	−951(3)	28(4)
	4390(3)	−1195(6)	−946(3)	28(4)
	4354(7)	−1222(13)	−996(8)	59(10)
	4356(2)	−1257(3)	−1001(2)	22(1)
N43(B)	5718(6)	−1681(11)	610(6)	70(8)
	5740(3)	−1643(6)	605(3)	36(4)
	5740(4)	−1635(6)	602(3)	34(4)
	5706(8)	−1648(15)	593(8)	63(10)
	5754(2)	−1656(3)	606(2)	24(1)

[a] $U_{eq} = {}^1/_3\sum_i\sum_j U_{ij}a_ia_ja^*_ia^*_j$.

same samples at 293 and 78 K; (2) X-band measurements on a polycrystalline copper-doped zinc sample between 4 and 450 K and Q-band measurements on the same sample at 293 K; (3) X-band measurements on a single crystal of the copper-doped zinc compound at 78 K (field rotation in three orthogonal planes) and between 40 and 300 K with the field in one crystal orientation.

Computer simulations of the spectra were carried out using a locally modified version of a program by Daul et al.[17] This program allows for rotation of tensors, addition of spectra, and inclusion of ligand hyperfine splittings.

Results and Discussion

The X-ray Structures. The structures of both the copper and the zinc complexes at all measurement temperatures belong to space group $P2_1/n$ with two independent pairs of centrosymmetric molecules per unit cell. Atomic parameters for the two independent MN_6 units, designated as sites A and B, are given in Table 2, and the geometries around the two metal ions, as illustrated for the zinc compound at room temperature, together with the atom labeling, are given in Figure 1. While the two geometries qualitatively appear to approach the idealized S_6 ($\bar{3}$) symmetry possible for the $Zn(mtz)_6^{2+}$ unit, the dimensions of the coordination polyhedra differ slightly, the ZnN_6 octahedron at site B being more regular than that at site A and, within the rather large esd's, having equivalent Zn−N distances at room temperature. At 100 K, the bond distance patterns change, site B showing a small, but significant, tetragonal elongation relative to the room-temperature structure, while site A exhibits a change from a (marginally significant) small tetragonal compression at 293 K to a more significant tetragonal elongation. These results suggest that the local-site strains are temperature dependent in the zinc complex and that their variation will thus be influential in determining the EPR spectra of the copper-doped complexes.

The relevant M−N distances for the zinc complex are given as part of Table 3, while those for the copper complex are given in Table 4. The N−M−N bond angles are close to 90°, varying from 88.10(12) to 91.90(12)° for both A and B sites in $Zn(mtz)_6^{2+}$ at 100 K and from 88.35(13) to 91.65(13)° for these sites in $Cu(mtz)_6^{2+}$ at 93 K. The metal ions for both sites lie in the planes of their respective mtz ligands, and the orientations of the three planes of each pair of *trans* ligands is such that they are almost mutually orthogonal.

The variations in the Cu−N distances on the two sites, although taking the same form as those for the zinc complexes, are considerably larger and differ markedly between site A and site B, reflecting the nature of the Jahn−Teller behavior at the two sites and the influence of the different site strains on this behavior. The geometry in the CuN_6(A) unit changes from slightly rhombic at 293 K to almost tetragonal, with Cu−N41 as the "long" bond, at 123 and 93 K. It appears that we are here dealing with a pulsating Jahn−Teller center that is concentrated mainly in one potential well.[18] The geometry changes in the CuN_6 unit at site B as the temperature is lowered are also indicative of a pulsating Jahn−Teller center. Here, however, the room-temperature rhombic geometry with the longer Cu−N43 bond changes at 123 and 93 K to a rhombic one in which Cu−N41 is the "long" bond. In this case, it is unlikely that the 93 K structure is the ultimate static low-temperature structure, since considerably smaller ligand **U** tensors, comparable to those found for the ZnN_6(B) unit at 100 K, would be expected.[19] In addition, the low-temperature EPR data (*vide infra*) cannot be interpreted in terms of a rhombic geometry.

The $M(mtz)_6^{2+}$ ions at both A and B sites are oriented with their pseudo−3-fold axes approximately parallel to the a^* axis, the angles of inclination of the M−N bonds to a^* ranging from 52.9(1) to 57.2(1)° for site A and from 50.0(1) to 61.2(1)° for site B. They pack, together with the BF_4^- ions, in a pseudo-trigonal arrangement in layers parallel to the (100) plane, and this is illustrated in Figure 2. The M(A)−M(B) and M(A)−M(A) [or M(B)−M(B)] distances in the plane vary from 10.558 (Cu) to 10.587 Å (Zn) and from 10.289 to 10.131 Å (b axis),

(17) Daul, C.; Schlapfer, C. W.; Mohos, B.; Ammeter, J.; Gamp, E. *Comput. Phys. Commun.* **1981**, *21*, 385.

(18) The description of the dynamic behavior of the A and B sites as pulsating follows the nomenclature introduced by Bersuker to describe the strong coupling situation where the system is in one of three configurations, performs vibrations around that configuration, and then rapidly switches to one of the other configurations (Bersuker, I. B. *The Jahn−Teller Effect and Vibronic Interactions in Modern Chemistry*; Plenum Press: New York, 1984). We suggest that the description, dynamic Jahn−Teller effect, be reserved for the case of a weak $E \otimes \epsilon$ coupling, where there is little or no warping of the potential surface and which behaves very differently both theoretically and experimentally from the strong coupling case. See: Ham, F. S. In *Electron Paramagnetic Resonance*; Geschwind, S., Ed.; Plenum Press: New York, 1972.

(19) In an attempt to obtain information on the geometry of this center at a lower temperature, a single-crystal neutron study at 20 K was undertaken. However, on cooling of the large crystals needed for such a study, the mosaic spread of the orientation reflections increased to unacceptable levels, and the project was abandoned.

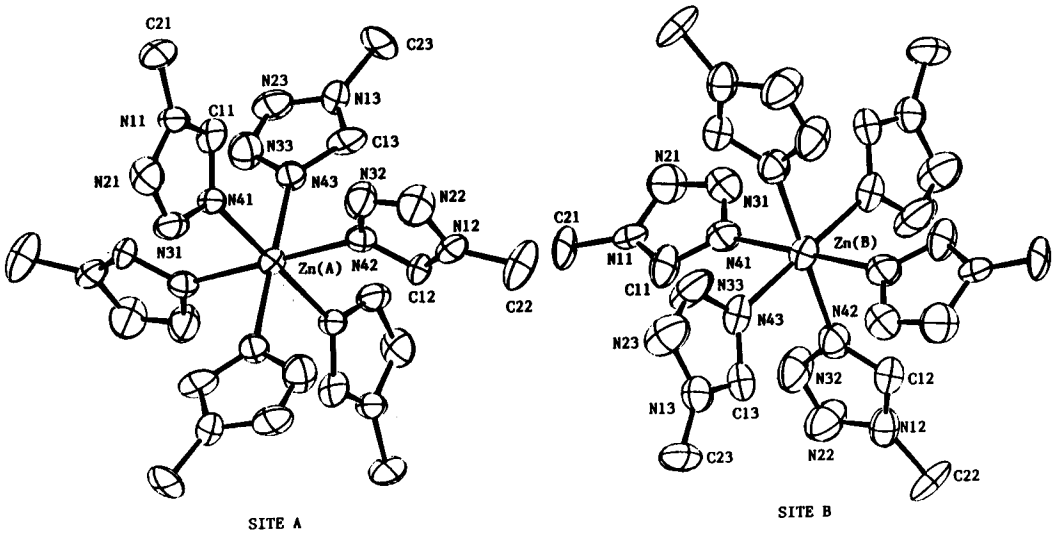

Figure 1. ORTEP projections of the two crystallographically inequivalent $Zn(mtz)_6^{2+}$ ions in the room temperature (293 K) structure of $Zn(mtz)_6(BF_4)_2$ viewed along the pseudo-3-fold axes and giving the atom labeling. The ellipsoids are at the 50% probability level.

Table 3. Zn−N Bond Distances and U^2 Values for Zn $(mtz)_6^2$

	bond	d_{obsd} (Å)	U^2_N(Å^2)[a]	U^2_{Zn}(Å^2)[a]	d_{calcd} (Å)[b]
		(A) $T = 293$ K			
site A	Zn−N41	2.181(9)	0.034(7)	0.037(1)	
	Zn−N42	2.142(9)	0.042(7)	0.046(1)	
	Zn−N43	2.174(9)	0.042(7)	0.046(1)	
	av	2.166(9)			
site B	Zn−N41	2.159(11)	0.050(9)	0.051(1)	
	Zn−N42	2.156(11)	0.070(9)	0.067(2)	
	Zn−N43	2.148(11)	0.068(9)	0.072(1)	
	av	2.154(11)			
		(B) $T = 100$ K			
site A	Zn−N41	2.194(3)	0.023(1)	0.021(0.2)	2.193
	Zn−N42	2.128(3)	0.026(1)	0.023(0.2)	2.134
	Zn−N43	2.153(3)	0.021(1)	0.020(0.2)	2.149
	av	2.158(3)			2.159
site B	Zn−N41	2.174(3)	0.031(2)	0.030(0.2)	2.171
	Zn−N42	2.157(3)	0.038(2)	0.040(0.3)	2.152
	Zn−N43	2.155(3)	0.034(2)	0.034(0.3)	2.158
	av	2.162(3)			2.160

[a] Values along the respective Zn−N bond vectors; the differences $\Delta U^2 = U^2_N - U^2_{Zn}$ are included in the calculations of the Jahn−Teller radii given for the $Cu(mtz)_6^{2+}$ complexes in Table 4. [b] Zn−N bond distances at 100 K as calculated via the crystal-strain model described in the text.

respectively, while the M(A)−M(B) interplanar distances (a/2) vary from ca. 9.1 Å at room temperature to 8.8 Å at low temperature.

In a rigorous trigonal arrangement ($P\bar{3}$) sites A and B would be required to be translationally equivalent. In the actual structure, however, the relative orientations of the two complexes about the a^* axis differ. The two cations A and B within the plane are in fact rather closely related by a non-space group required 2_1 axis parallel to z at $0,{}^1/_4, 0$ or alternatively, since the two sites have $\bar{1}$ symmetry, a b-glide plane at $x = {}^1/_4$. The locations of these pseudoelements are indicated in Figure 2. The axis and glide plane "relate" ligands 1, 2, and 3 on site A to the correspondingly numbered ligands on site B or to their inversion equivalents. One consequence of the packing arrangement is that the angle between the bond vectors M−N41(A) and M−N41(B) is *ca.* 84° for sites A and B within the (100) layer and 78° for sites in neighboring layers, so that, at low temperature, the two elastic dipoles for the two sites are approximately antiferrodistortively (AF) ordered.

Interpretation of the Ligand U Tensors. In this section we use a model incorporating the experimental metal−ligand bond distances and their respective **U** tensors to calculate values for the Jahn−Teller radius, ρ_{JT}, and the occupation probabilities of the potential wells. The model can be applied to all three independent ligand atoms, the local z axes being taken along each of the three individual metal−ligand bond vectors in turn to yield the respective probabilities, p_i, p_j, and p_k for the three wells. The basic formulas employed are developed elsewhere[10] and summarized here as follows:

$$\rho_\pi = -\frac{\langle Q_\theta \rangle}{2} + 3\left(\frac{\langle Q_\theta \rangle^2}{4} + {}^2/_3\langle U^2 \rangle\right)^{1/2} \quad (1)$$

$$p = {}^1/_3 + {}^2/_3\langle Q_\theta \rangle/\rho_{JT} \quad (2)$$

where: $\langle Q_\theta \rangle = (2r_z - r_x - r_y)/\sqrt{3}$; (normal coordinate of octahedron); r_x, r_y, and r_z are the experimental metal−ligand bond lengths (in Å), and $\langle U^2 \rangle$ is the net U value of the ligand atom (in Å^2) in the z direction. In its application to the refinement results for the $M(mtz)_6^{2+}$ structures, the model yields a total of 18 values for ρ_{JT}, three values for each of the two crystallographically independent copper atoms at three different measurement temperatures. These values, incorporating corrections provided by the zinc compounds, are given in Table 4.[20] The scatter among the sets of three values is reasonably small, and the values are essentially independent of crystal environment, although there is some indication that the Jahn−Teller radii become slightly larger at lower temperature. The overall average, 0.41(3) Å, is significantly larger than those found for most other complexes containing the CuN_6 moiety, typically *ca.* 0.32 Å.[21] However, the majority of these complexes have three bidentate or two tridentate ligands, and it is likely that such species will have higher force constants for the E_g vibration due to the steric constraints provided by the ligands. Support for this is available in Table 12 of ref 21.

Examining the probabilities for the two Jahn−Teller centers, we see that the copper ion on site A behaves in a "normal" way. At room temperature, two of the three wells are occupied, one [88(5)%] being heavily preferred to the second [16(3)%].

(20) While in the present analysis the X-ray results for the zinc structures were used, it does appear that calculations using the data for copper complexes alone also give reasonable values for the Jahn−Teller radii and population distribution.

(21) Ammeter, J. H.; Burgi, H. B.; Gamp, E.; Meyer-Sandrin, V.; Jensen, W. P. *Inorg. Chem.* **1979**, *18*, 733.

Table 4. Cu−N Bond Distances, U^2 Values, Jahn−Teller Radii, and Potential Well Populations for $Cu(mtz)_6^{2+}$

	bond	d (Å)	U^2_N (Å^2)[a]	U^2_{Cu} (Å^2)[a]	ΔU^2 (Å^2)[b]	ρ_{JT} (Å)[c]	p[c]
			(A) $T = 293$ K				
site A	Cu−N41	2.334(8)	0.053(5)	0.042(1)	0.014(6)	0.40(3)	0.86(5)
	Cu−N42	2.024(8)	0.037(5)	0.041(1)	0.000(6)	0.44(5)	0.00(5)
	Cu−N43	2.092(8)	0.045(6)	0.035(1)	0.014(6)	0.38(4)	0.16(3)
	av	2.150(8)				0.41(4)	
site B	Cu−N41	2.114(9)	0.077(6)	0.048(1)	0.031(7)	0.45(4)	0.29(2)
	Cu−N42	2.083(10)	0.084(6)	0.060(1)	0.021(7)	0.42(4)	0.20(3)
	Cu−N43	2.191(10)	0.091(6)	0.073(1)	0.022(7)	0.35(5)	0.54(2)
	av	2.129(10)				0.41(4)	
			(B) $T = 123$ K				
site A	Cu−N41	2.378(5)	0.017(3)	0.018(.6)	0.000(4)	0.41(2)	0.99(4)
	Cu−N42	2.012(5)	0.023(3)	0.017(.6)	0.003(4)	0.47(3)	0.01(3)
	Cu−N43	2.038(5)	0.014(3)	0.012(.6)	0.001(4)	0.37(4)	0.01(3)
	av	2.143(5)				0.42(3)	
site B	Cu−N41	2.205(5)	0.044(4)	0.018(.7)	0.025(5)	0.36(4)	0.57(2)
	Cu−N42	2.055(5)	0.043(4)	0.031(.7)	0.014(5)	0.42(4)	0.12(2)
	Cu−N43	2.135(5)	0.053(4)	0.030(.7)	0.023(5)	0.38(4)	0.32(1)
	av	2.132(5)				0.39(4)	
			(C) $T = 93$ K				
site A	Cu−N41	2.379(5)	0.018(3)	0.016(.6)	0.000(4)	0.41(2)	1.00(4)
	Cu−N42	2.014(5)	0.018(3)	0.016(.6)	0.000(4)	0.44(3)	0.00(3)
	Cu−N43	2.036(5)	0.014(3)	0.015(.6)	0.002(4)	0.37(4)	0.00(3)
	av	2.143(5)				0.41(3)	
site B	Cu−N41	2.211(6)	0.049(4)	0.019(.6)	0.029(5)	0.40(4)	0.57(2)
	Cu−N42	2.046(6)	0.044(4)	0.031(.6)	0.015(5)	0.44(3)	0.12(2)
	Cu−N43	2.126(6)	0.057(4)	0.028(.6)	0.029(5)	0.42(3)	0.33(1)
	av	2.128(6)				0.42(3)	

[a] Values along the respective Cu−N bond vectors. [b] Values of $U^2_N - U^2_{Cu}$ including the corrections for the corresponding Zn−N bonds, derived from the data in Table 3. [c] Jahn−Teller radii and potential well populations obtained from eqs 1 and 2.

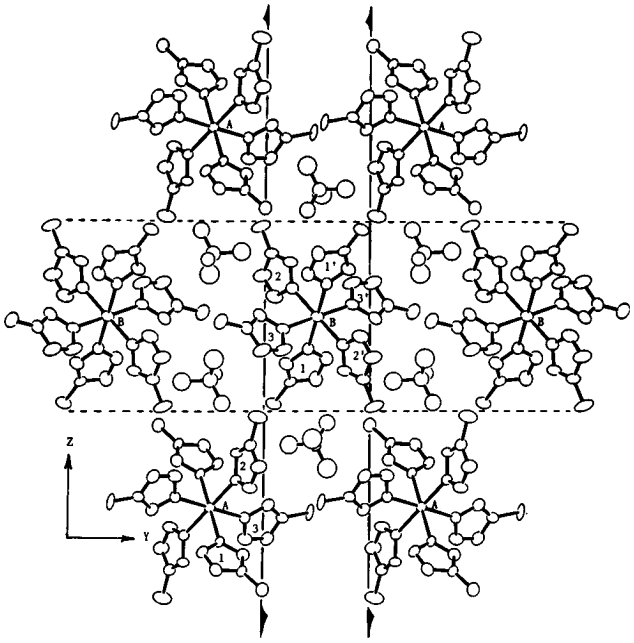

Figure 2. Projection onto (100) of one layer of the structure of $Zn(mtz)_6(BF_4)_2$. The locations of the pseudosymmetry elements relating the complex ions on sites A (0, 0, 0) to those on sites B (0, $^1/_2$, $^1/_2$) are indicated by full (2_1 axes) and broken (*b*-glide) lines. These elements respectively relate ligands 1 on (A) to 1 on (B), 1 on (A) to 1′ on (B), etc.

As the temperature is lowered, the dynamic equilibrium shifts, such that the second well is depopulated, until, at 93 K, effectively only the one well is occupied, giving a geometry for the CuN_6 group which is almost D_{4h}.

The copper on site B, on the other hand, behaves in a different way. As is evident from the probabilities, which are closer to $^1/_3$, the three wells are closer in energy, giving a structure in which the copper atoms are pulsating between the wells at 293 K. When the temperature is lowered, as noted earlier, the most elongated bond changes from Cu−N43 at 293 K to Cu−N41 at low temperature and the probabilities change accordingly. Clearly the well having the lowest energy at low temperature is not the same as that at 293 K, and a precedent for similar behavior is found for the recently reported low-temperature structure of $Cu(ttcn)_2(BF_4)_2(MeCN)_2$.[9,22] We thus conclude that, for the B sites, the angular potential is temperature dependent and that it changes as the local site strain for this site changes with temperature. It has already been noted that the site strains for the nonactive zinc complex appear to be temperature dependent, and the behavior exhibited by the undiluted copper complex suggests that local-site strain changes, very similar in form to those for the zinc complex, are operative here and account, at least in part, for the changes in the relative order of the energies of the three wells in the potential surface.

An additional factor also probably playing a role is the weak elastic interaction between the A and B sites. As mentioned earlier, the "long" bonds at low temperature, Cu−N41(A) and Cu−N41(B), are almost orthogonal, so that the distorted octahedra with these bonds as tetragonal axes are approximately antiferrodistortively ordered. On the basis of a wide variety of results from other systems, the antiferrodistortive arrangement of neighboring Jahn−Teller-active sites appears to be favored and to occur more frequently than the ferrodistortive one.[9,11,23,24]

(22) The slightly rhombically distorted CuS_6 geometry found at room temperature in crystals with space group *Pbca* (Setzer, W. N.; Ogle, C. A.; Wilson, G. S.; Glass, R. R. *Inorg. Chem.* **1983**, *22*, 266) is replaced at 117 K by two crystallographically inequivalent (but geometrically equivalent) rhombically distorted geometries in space group $P2_1/c$.[9] The bond lengths and angles of both room- and low-temperature structures are essentially the same, but interestingly the two independent low-temperature cations and the room-temperature cation are mutually antiferrodistortively arranged; *i.e.*, the three marginally longer Cu−S bonds are all orthogonal. The **U** tensor model described here was also applied to the two CuS_6 entities in the 117 K structure, and the Jahn−Teller radii were found to be 0.32 and 0.34 Å.

(23) Keijzers, C. P.; McMullan, R. K.; Wood, J. S.; Van Kalkeren, G.; Srinivasan, R.; deBoer, E. *Inorg. Chem.* **1982**, *21*, 4275.

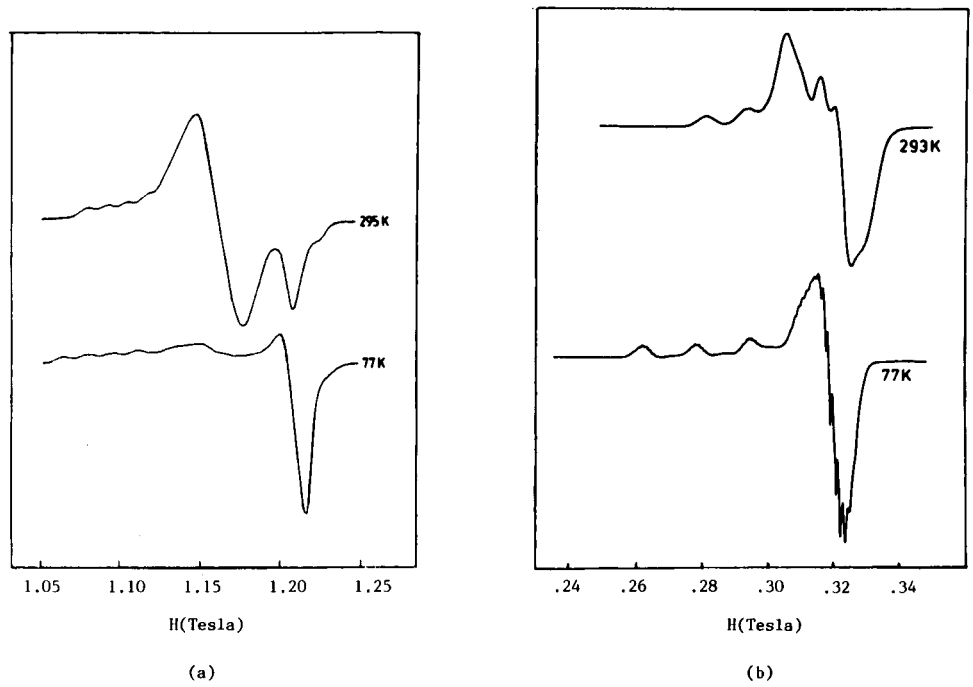

Figure 3. (a) Q-Band EPR spectra of polycrystalline $Cu(mtz)_6(BF_4)_2$ at 293 and 77 K. (b) X-Band EPR spectra of polycrystalline $Zn(mtz)_6(BF_4)_2$: Cu^{2+} at 293 and 77 K.

Site B then changes from one in which the long Cu−N43 bonds have a partial AF orientation to the elongated octahedron on site A at room temperature, to a distribution at 93 K where the AF ordering is more extensive. This can be understood in terms of the change in the Cu−N41(A) bond distance with temperature, for the AF interaction of this elastic dipole with Cu−N41(B) will increase in size with decreasing temperature and probably more so than the elastic interaction of Cu−N41(A) with Cu−N43(B).

Paralleling the analysis of the individual **U** tensor data for the CuN_6 and ZnN_6 moieties, we also carried out rigid-body analyses of the **U** tensor data for the complete ligands following the TLS procedure of Schomaker and Trueblood.[25] The results of these calculations indicate that, for both copper and zinc complexes, the ligands behave essentially as independent rigid bodies at all temperatures and that the Jahn−Teller activity of the copper centers is incorporated primarily into the ligand translational (**T**) tensors. While for site A these tensors are closely comparable to those for the zinc complex, for site B they are significantly different at both 93 and 293 K, the components parallel to the Cu−N41 and Cu−N43 vectors being appreciably larger than those normal to the bonds, a result consistent with the presence of a Jahn−Teller-active site with primarily two occupied minima in the potential surface.

EPR Experiments on Powders and Single Crystals. All EPR spectra measured can be described using the standard spin Hamiltonian

$$H = H\cdot g\cdot S + S\cdot A_{Cu}\cdot I_{Cu} + S\cdot A_N\cdot I_N \qquad (3)$$

with $S = {}^1/_2$ and $I_{Cu} = {}^3/_2$ for copper and $I_N = 4$ for four nitrogen atoms. Since the prepared compounds contain naturally abundant copper, this gave rise to problems in the assignment of the ligand hyperfine splittings.

The distances between copper ions are rather large (*ca.* 8.9 Å for the shortest interlayer distance) so that magnetic dipole−dipole and exchange interactions are apparently small and standard four-line spectra result, with line widths of about 5 mT. At 293 K, both Q- and X-band spectra of polycrystalline samples of $Cu(mtz)_6^{2+}$ show a superposition of signals from two copper species, one with a large *g* anisotropy and one with a much smaller anisotropy. The Q-band spectrum is illustrated in Figure 3a. This is consistent with the presence of two different Jahn−Teller sites as revealed by the X-ray diffraction results at 293 K. When the temperature is lowered, the near-isotropic signal gradually disappears, and the resulting spectrum below l00 K is one that apparently arises from a single Jahn−Teller site of tetragonal symmetry, namely an axial spectrum with a *g* anisotropy slightly larger than that of the anisotropic signal seen at room temperature.

Compared to those for the pure compound, the spectra for powder samples of the copper−doped zinc compound have narrower line widths and the ligand hyperfine splittings are resolved in spectra recorded below 170 K. However, the temperature dependence of the spectra and the smaller anisotropy of the room temperature signal are entirely analogous to those for the pure compound, as is indicated by Figure 3b, and so we conclude that elastic interactions in the pure compound are not important in determining the EPR transitions in the complex on site B, the three minima in its potential surface being mainly determined by the nonrandom strain induced by the crystal site being lower than the C_{3v} symmetry of the potential.

The powder spectra below 100 K indicate that there is only one type of copper site present in the compound, so that evidently the lowest minimum for both copper centers is close to $\phi = 0$, $2\pi/3$, or $4\pi/3$ radians, although the magnitudes of the E_g fields will be different for the two centers.

Assuming axial **g** and hyperfine tensors, these low-temperature (77 K) spectra yield the following values: $g_{\|} = 2.300(5)$ and $g_{\perp} = 2.068(5)$, for copper, $A_{\|} = 17.7$ (5) and $A_{\perp} < 2.0$ and, for nitrogen, $A_{\|} = 1.3(2)$ and $A_{\perp} = 1.5(5)$ (all hyperfine values $\times 10^3$ cm^{-1}). Using these results, the probabilities p_i etc. from Table 4 were used to simulate the EPR spectra measured at 293 K. For this purpose, it was assumed that the wells and the potential energy surfaces for both centers are

(24) Crama, W. J.; Maaskant, W. J. A. *Physica* **1983**, *121B*, 219.
(25) Schomaker, V.; Trueblood, K. N. *Acta Crystallogr.* **1968**, *B24* , 63.

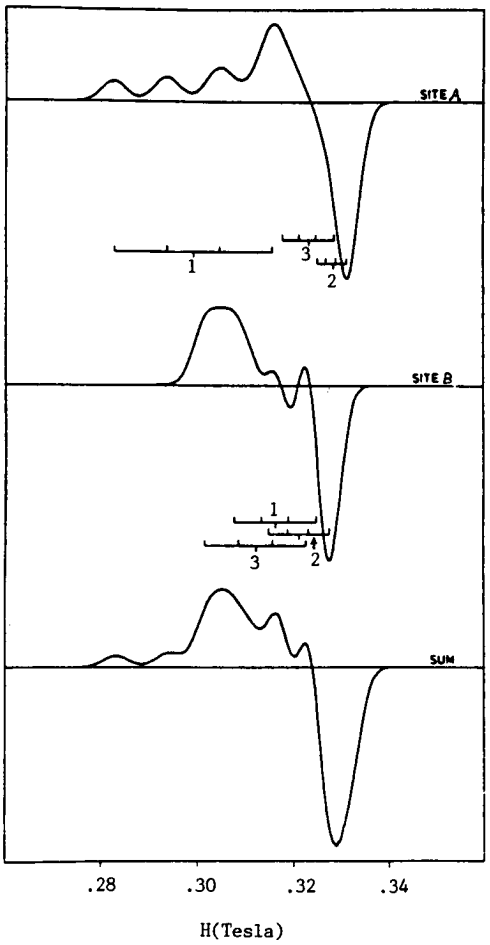

Figure 4. Calculated X-band EPR spectra of polycrystalline $Cu(mtz)_6(BF_4)_2$ at 293 K. The sum spectrum is obtained by the addition of the calculated spectra for sites A and B with equal weighting, and it can be compared with the experimental spectrum for $Zn(mtz)_6(BF_4)_2$:Cu^{2+} given in Figure 3b. The motionally averaged g and A values for the resonances centered at 1, 2, and 3 for each site were calculated (eq 4) as follows: for site A, $g_1 = 2.268$, $g_2 = 2.068$, $g_3 = 2.100$, $A_1 = 15.4$, $A_2 = 1.5$, and $A_3 = 3.8$; for site B, $g_1 = 2.147$, $g_2 = 2.114$, $g_3 = 2.175$, $A_1 = 7.0$, $A_2 = 4.7$, and $A_3 = 9.0$ (all A values $\times 10^{-3}$ cm^{-1}).

located very close to 0, $2\pi/3$, or $4\pi/3$, so that equations of the form given in (4) can be used to calculate the motionally averaged **g** and **A** tensors: The resulting spectra based on the

$$g_i = p_i g_{||} + (p_j + p_k) g_{\perp} \qquad (4)$$

spin-Hamiltonian in (3), assuming equal contributions for the two copper centers, are given in Figure 4. In view of the uncertainties concerning the transition line shapes, the simulated spectrum fits reasonably well to the experimental one depicted in Figure 3b, thus supporting the proposed model.

Although complete X-band spectra for three mutually orthogonal planes of a doped single crystal were recorded at 78 K, their interpretation was extremely difficult due to extensive overlap of the transitions, and it did not prove possible to obtain more accurate **g** and **A** tensors. However, it was possible to select a crystal orientation which gave spectra whose low-field parts were determined solely by the complex on site B, Figure 5 and gives selected spectra for this orientation at temperatures from 50 to 180 K. It can be seen that in a small temperature range around 140 K, the spectra for both a motionally averaged and a static site occur together, indicating that the pulsating CuN_6(B) centers are gradually shifting their equilibrium toward a tetragonally elongated configuration. Below *ca.* 100 K, the contributions of the potential wells are no longer motionally

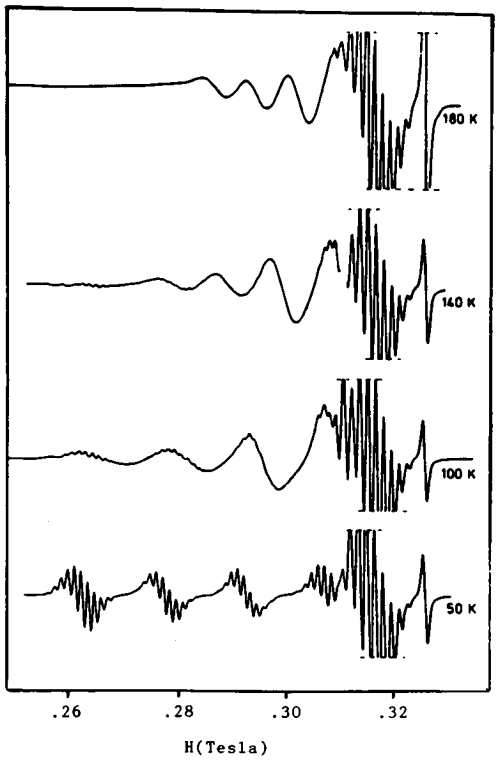

Figure 5. X-Band EPR spectra at different temperatures for a single crystal of $Zn(mtz)_6(BF_4)_2$:Cu^{2+}. The crystal orientation relative to the magnetic field is the same for all spectra. The spectrum at 140 K shows both a motionally averaged signal and an anisotropic signal having ligand hyperfine structure. The highest field resonance is due to a g marker ($g = 2.0065$).

averaged, in agreement with the result obtained from the low-temperature powder spectra, which show an axial **g** tensor resulting from the trapped out contributions of the three wells at site B, together with that from site A.

Combining the results of the X-ray and EPR experiments, we may then summarize the models for the Jahn−Teller activity of the two Cu $(mtz)_6^{2+}$ complexes as follows:

(1) The CuN_6 unit on site A is a rapidly pulsating Jahn−Teller center having one potential well that has a much lower energy than the other two. Although the X-ray results indicate a small but significant population for one of the other wells, and the slightly smaller anisotropy in the **g** tensor is in accord with this, the geometry of this center is close to tetragonally elongated at room temperature. This also appears to be the case at temperatures appreciably above 293 K, on the basis of EPR spectra recorded at these higher temperatures. On lowering of the temperature, the preference for the lowest potential well increases so that below 100 K its population is 100% and the CuN_6(A) unit becomes static.

Very similar comments can be made regarding the copper ion on site A in the zinc host complex. The small tetragonal compression exhibited by the host crystal is consistent with the occupation of two potential wells with one well more heavily preferred and so leads to a motionally averaged EPR spectrum for the doped sample giving a somewhat smaller g anisotropy than the corresponding spectrum at 78 K.

(2) In contrast, the CuN_6 unit on site B is pulsating at 293 K with an appreciable population in all three potential wells, both in the pure compound and in the compound doped into the zinc host. To within the esd's, the latter shows almost zero site strain and so we anticipate nearly equal populations of the three wells for the doped CuN_6(B) unit, consistent with the appearance of an almost isotropic EPR spectrum.

On cooling, the equilibrium among the three wells changes, until in the region of 130 K, the EPR results from the doped single crystals indicate a center where the pulsations are slowed to below 1 GHz−the limit for motional averaging. For the pure complex, the potential well populations, as deduced from the 123 and 93 K X-ray data, change very little in this temperature region, and so also are in agreement with a model in which motional averaging is minimal below *ca.* 100 K. At this temperature, the pulsations are therefore trapped out, so that the observed X-ray structure for the B centers is one averaged over Jahn−Teller sites having tetragonal geometries for the CuN_6 units and one for which, on the basis of **U** tensor analysis, the octahedra are elongated along *x*, *y*, and *z*, respectively, (i.e. bonds to N41, N43, and N42) in an approximate 5:3:1 ratio.

While in standard crystallographic terminology this would probably be described as a thermally disordered structure, and certainly the larger than expected **U** tensors are consistent with this description, it might also be depicted as a "glassy" arrangement of Jahn−Teller centers, since there is no imposed long-range order relating the arrangement of the three differently elongated octahedra according to the space group symmetry.

The prediction that a diluted Jahn−Teller system might behave as a glass was made some years ago, and the term was introduced to describe the situation where frozen-in random strain fields lead to a disordered arrangement for the alignment of the Jahn−Teller-active centers.[26] In a concentrated crystal, where cooperative effects between the centers are significant and larger than the random strains, there is generally a phase transition as the temperature is lowered, leading to ferro- or antiferrodistortive ordering accompanied by a change in crystal structure. Although the $Cu(mtz)_6^{2+}$ system is nondilute, the cooperative effects between the Cu(B) sites are apparently sufficiently weak that the random strains, probably augmented by the (disordered) BF_4^- ions and other crystal defects, are more significant and, taken with the near-equivalence of the three wells for the B sites, lead to a lack of long-range order for these sites.[27]

Effect of Crystal Strain on the Jahn−Teller Behavior. In the previous sections we have described how the local-site strains of the octahedra in the zinc complex appear to be temperature dependent and have discussed how similar strains seem to be operative in the copper complex and can account, at least partially, for the bond length variations observed for the two Jahn−Teller-active sites. Although these local strains are quite different for the two sites, we have sought to understand if they have a common origin and can be explained in terms of a single strain field arising from the placement of the $M(mtz)_6^{2-}$ ions, with idealized S_6 symmetry, along with the BF_4^- ions, in the lower symmetry monoclinic cell.

In this section we therefore examine the effect of a single strain field of monoclinic (2/*m*) symmetry on the geometries of the two Jahn−Teller-inactive ZnN_6 octahedra, assuming that the deviations from the S_6 symmetries with equal Zn−N bond lengths can be used to model the strain. We emphasize that the source of this strain is not due to any external applied stress but is assumed to arise solely from the close-packing requirements of the monoclinic cell.

The strain e_i in a general direction in a crystal, defined by a unit vector **X**, can be written as[28]

$$e_i = \mathbf{X}_i^{\mathrm{t}}\mathbf{E}\mathbf{X}_i \tag{5}$$

where the components of the column vector $\mathbf{X}_i$ are the direction cosines l_i, m_i, and n_i relative to an orthogonal axis system and **E** is a second rank tensor describing the strain. In this application, the vectors **X** are taken along the Zn−N bond directions, and the orthogonal axes, as *a**, *b*, and *c*, while for 2/*m* symmetry and with the totally symmetric deformations of the octahedra omitted, **E** can be written as

$$\mathbf{E} = \begin{bmatrix} \epsilon_{11} & 0 & \epsilon_{13} \\ 0 & \epsilon_{22} & 0 \\ \epsilon_{13} & 0 & -(\epsilon_{11}+\epsilon_{22}) \end{bmatrix}$$

Using the six experimental bond length deformations from octahedral (or S_6) symmetry as reflecting the strains, e_i, the following equations are obtained from (5):

$$(l_i^2 - n_i^2)\epsilon_{11} + (m_i^2 - n_i^2)\epsilon_{22} + 2l_in_i\epsilon_{13} = \epsilon_i \quad (i = 1, ..., 6) \tag{6}$$

with e_i calculated as $(d_i - \bar{d})/\bar{d}$ where $\bar{d}$ is the average bond length for the (presumed undistorted) octahedron. Least-squares treatment of (6) gives an almost axial tensor with principal values 0.084(12), −0.047(10), and −0.037(12), oriented with its main axis almost parallel to *a** (inclined at *ca.* 6°). Given the simplicity of the model, it is gratifying that **E** is oriented such that its maximum component is in the direction roughly normal to the (100) plane. In this direction, on the basis of relative interionic distances, the Coulombic forces between $M(mtz)_6^{2+}$ and BF_4^- will be weaker than those in the plane (at least 8.9 Å compared to 5.8 Å), and this "softness" is reflected in the temperature dependence of the *a* axis which decreases by *ca.* 2.5% between room temperature and 90 K, compared to smaller changes in *b* and *c*.

While the main axis of the strain tensor is also approximately aligned with the pseudo-3-fold axes of the MN_6 octahedra, and can thus be qualitatively characterized as a t_{2g} strain, this orientation is only approximate, and it is possible to resolve the strain into components along the bond and (1, 1, 1) directions, i.e. into e_g and t_{2g} components, respectively. This reveals that site A, and in particular the Zn−N41 bond, experiences somewhat larger e_g components than site B, for which the angles between the major axis of the strain and the Zn−N bond vectors are closer to 54.75°. In terms of its capacity to deform the MN_6 octahedra in an e_g sense, it therefore seems that this crystal packing strain has a greater impact on site A than on site B, and using the value for **E**, we find that the calculated deformations of the two octahedra agree quite well with the experimental values and, for low temperature, reflect the observed local strains. The resulting calculated Zn−N bond distances for the two sites are given in Table 3.

In order to evaluate the consequences of the distortions of the MN_6 octahedra for the Jahn−Teller behavior at the copper sites, the calculated strains need to be expressed as the E_g symmetrized strains

$$e_\theta = (2e_z - e_x - e_y)\bar{d}/\sqrt{3}$$

$$e_\epsilon = (e_x - e_y)\bar{d}$$

and using the calculated values, one obtains $(e_\theta, e_\epsilon) = (0.060,$

(26) Mehran, F.; Stevens, K. W. H. *Phys. Rev.* **1983**, *B27*, 2899

(27) Crystals of the (pyridine oxide)copper complex Cu $(PyO)_6(ClO_4)_2$ grown from DMF solution also appear to form a Jahn−Teller glass system at temperatures less than 40 K.[23] Here the strain centers are provided by the partially substituted complexes $Cu(PyO)_4(DMF)_2^{2+}$, and these crystals exhibit different EPR and structural behavior very different from those of crystals grown from other solvents.

(28) Nye, J. F. *Physical Properties of Crystals. Their Representation by Tensors and Matrices*; Clarendon Press: Oxford, England, 1960.

0.014 Å) for site A and (0.018, 0.006 Å) for site B. Assuming that these E_g strains are also active in the copper complex, and taking the relative shifts of the three energy minima of the warped Mexican hat potential to be proportional to the strain energy term $e_\theta \cos \phi + e_\epsilon \sin \phi$ for the minima at $\phi = 0, 2\pi/3$, and $4\pi/3$, we find that the *relative* strain energy terms for these minima are −0.042 (N41), −0.018 (N42), and 0.060 (N43) for the copper at site A and −0.014 (N41), −0.004 (N42), and 0.018 (N43) for the ion at site B, thus confirming that the relative energy differences between the minima are significantly larger at the A than at the B site. Using this simple model, we then see that the actual energy levels of the individual Cu(B) centers will probably be very sensitive to any additional strains of a random nature, such as those arising from impurities or disordered BF_4^- ions, so that the description of the low-temperature structure of these centers as "glassy" appears to be appropriate.

Summary

Crystals of the Jahn−Teller-active complex $Cu(mtz)_6(BF_4)_2$ present a rather special situation in that they contain CuN_6 centers located on two inequivalent sites in a monoclinic unit cell, each site exhibiting Jahn−Teller distortions but in different ways. While the Jahn−Teller radii are large and are the same for both $Cu(mtz)_6^{2+}$ species, in keeping with the general conclusions of Ammeter and co-workers for systems containing CuN_6 and CuO_6 centers,[21] the variable-temperature X-ray and EPR data show that the three energy minima in the distorted Mexican hat potential surface are much more equivalent for one site than for the other. This variability in Jahn−Teller behavior for the two sites is attributable to differences in the local low-symmetry strains, which are also temperature dependent, rather than to differences in the symmetric warping energies, which would in fact be expected to be very similar for the two complexes. Generalizing from this example and from our reasonably successful attempt at modeling the strains in terms of a crystal "packing" strain, we feel that the variable-temperature behavior of many CuX_6 coordination centers is determined by the E_g symmetric strain fields, rather than by the magnitude of the O_h symmetric warping energies.

The other result obtained from this study that is of some significance is the apparent presence in the $Cu(mtz)_6(BF_4)_2$ crystals of a disordered or "glassy" arrangement for half of the CuN_6 sites at temperatures below which the inter-well pulsations are trapped out. This contrasts with the more usual situation where the cooperative ordering between Jahn−Teller centers normally leads to a first-order phase change below such a transition point.

Acknowledgment. We are grateful to the late Dr. G. C. Verschoor, who carried out some of the initial crystallographic work on $Cu(mtz)_6(BF_4)_2$. Thanks are also expressed to Dr. R. A. G. de Graaf and Drs. Syb Gorter for assistance with the X-ray data collections, to Frans Hulsbergen and M. Welter for help with the EPR experiments and computer simulations, and to Dr. Kees Keijzers (University of Nijmegen) for recording the Q-band spectra of several samples.

Supporting Information Available: Tables S1−S6, listing complete crystallographic information, atomic coordinates, anisotropic thermal parameters, H atom coordinates, and bond distances and bond angles within ligands for $Cu(mtz)_6(BF_4)_2$ and $Zn(mtz)_6(BF_4)_2$ (14 pages). Ordering information is given on any current masthead page.

IC950315T